Error Analysis for Dielectric Spectroscopy using Shielded Open-Circuited Coaxial Lines of General Length

WAYMOND R. SCOTT, JR., MEMBER, IEEE, AND GLENN S. SMITH, FELLOW, IEEE

Abstract—**The shielded open-circuited coaxial line of general length is studied in detail as a sample cell for broad-band measurements of the dielectric permittivity. This cell is a section of transmission line with the center conductor abruptly terminated. The dielectric material to be measured fills the coaxial section of the cell and extends beyond the center conductor into the tube formed by the outer conductor of the transmission line.**

The inverse function for obtaining the permittivity of the sample from the measured input admittance of the cell is multivalued. The error in the measured permittivity caused by passing onto the wrong branch of the inverse function is analyzed, and a procedure that can prevent passage onto the wrong branch is developed. The error in the measured permittivity due to the inaccuracies in the instrumentation is also analyzed. Contour graphs are constructed that quantify the effects of this error on the measured permittivity. This error is shown to be largest when the combination of frequency, sample length, and sample permittivity place the measured normalized admittance near a branch point of the inverse function.

The permittivities of several primary alcohols were measured with the open-circuited sample cell. The measured relaxation spectra for these alcohols are used to demonstrate the usefulness of the error analysis.

I. Introduction

THE coaxial transmission line has been used as a sample cell in dielectric measurements for many years. In the earliest techniques, the input impedance of a section of transmission line was measured and used to infer the permittivity of the sample filling the line. The length of the sample, its position, and the impedance terminating the line were chosen to provide the best accuracy at each frequency being used. For example, an electrically thin sample was placed approximately one-quarter of a free-space wavelength from a short-circuit termination. These techniques are described in the book by von Hippel [1].

Over the last twenty years, automated instrumentation has become commercially available that can measure impedance over an ever increasing range of frequencies. This instrumentation consists primarily of automated network analyzers and automated time-domain reflectometers [2]–[6]. For optimum use of this instrumentation in dielectric measurements using coaxial sample cells, it is not practical to adjust the length of the sample or the termination to obtain the best performance at each frequency. Thus it is necessary to understand in detail the problems that exist when a single coaxial sample cell of fixed geometry is used over a very broad frequency range.

The coaxial sample cell shown in Fig. 1 is a section of transmission line with the center conductor abruptly terminated. The dielectric material to be measured fills the coaxial section of the cell and extends beyond the center conductor into the tube formed by the outer conductor of the transmission line. This cell is particularly useful for measuring the dielectric parameters of liquids and particulate matter, since the material is easily placed in the cell through the open end. Cells of this form have been used at the National Bureau of Standards for measuring the dielectric parameters of soils and agricultural materials [7].

In this paper, the coaxial sample cell shown in Fig. 1 is studied in detail. The inverse function for obtaining the permittivity of the sample from the measured input admittance of the cell is multivalued. The error in the measured permittivity caused by passing onto the wrong branch of the inverse function is analyzed, and a procedure that can prevent passage onto the wrong branch is developed. The error in the measured permittivity due to the inaccuracies in the instrumentation is also analyzed. This error is shown to be largest when the combination of frequency, sample length, and sample permittivity place the measured normalized admittance near a branch point of the inverse function.

II. The Inverse Function

The input admittance of a section of an ideal coaxial transmission line terminated with a perfect open circuit and filled with a linear, homogeneous, isotropic dielectric material is

$$Y(j\omega, \tilde{\epsilon}_r) = Y_o \sqrt{\tilde{\epsilon}_r} \tanh (j\omega \sqrt{\tilde{\epsilon}_r}\, l/c),^{1} \qquad (1)$$

where Y_o is the characteristic admittance of the empty

Manuscript received March 25, 1985; revised July 9, 1985. This work was supported in part by the Joint Services Electronics Program under Contracts DAAG29-81-K-0024 and DAAG29-84-K-0024, and by a Specialized Research Equipment Grant from the National Science Foundation, ENG77-17200. W. R. Scott was the recipient of a TRW Foundation Augmentation Fellowship during the term of this research.

The authors are with the School of Electrical Engineering, Georgia Institute of Technology, Atlanta, GA 30332.

IEEE Log Number 8607864.

[1]The TEM mode is assumed to be the only propagating mode in the coaxial line, and all waveguide modes are assumed to be cutoff in the hollow tube extending beyond the center conductor.

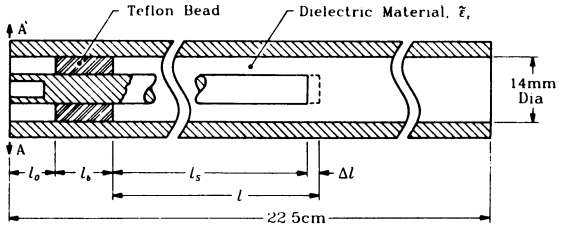

Fig. 1. The open-circuited coaxial sample cell.

transmission line, $\tilde{\epsilon}_r$ is the complex effective relative permittivity of the material filling the line, c is the speed of light in free space, and l is the length of the transmission line. The material is assumed to be nonmagnetic, and a harmonic time dependence of $e^{j\omega t}$ is used. After introducing the normalized admittance

$$W = \frac{j\omega l}{c} \frac{Y(j\omega, \tilde{\epsilon}_r)}{Y_o} \tag{2}$$

and the normalized propagation constant

$$S = j\omega \sqrt{\tilde{\epsilon}_r}\, l/c \tag{3}$$

(1) becomes

$$W = f(S) = S \tanh (S). \tag{4}$$

The permittivity $\tilde{\epsilon}_r$ is to be determined from the measured input admittance Y over a broad range of frequencies. The procedure is to obtain W from Y by (2), then to compute S from W by inverting (4), and finally to determine $\tilde{\epsilon}_r$ from S by (3):

$$\tilde{\epsilon}_r = -(Sc/l\omega)^2. \tag{5}$$

In the remainder of this section, the construction of the inverse of (4) is described, and the problems that arise due to the singularities in the inverse function are discussed.

The function $f(S)$ has simple poles at $S = j(2n + 1)\pi/2$, $n = 0, \pm 1, \pm 2, \pm 3, \cdots$; simple zeros at $S = jn\pi$, $n = \pm 1, \pm 2, \pm 3, \cdots$; and a double zero at $S = 0$. The function $f(S)$ is single valued, but the inverse function $f^{-1}(W)$ is multivalued. The branch points W_{bi} of the inverse function occur at the points S_{bi} at which the first derivative of $f(S)$ is zero; therefore, the branch points can be determined from the solutions S_{bi} of

$$df(S)/dS = d[S \tanh (S)]/dS = 0$$

or

$$2S = -\sinh (2S). \tag{6}$$

Equation (6) has an infinite number of solutions; thus the inverse function has an infinite number of branch points. The branch points are all of first order, i.e., $d^2f(S)/dS^2 \neq 0$ at $S = S_{bi}$. Since the branch points are of the first order, the inverse function has the behavior $[W - W_{bi}]^{1/2}$ near W_{bi}.

The inverse function can be made to appear single valued by the use of a Riemann surface [8]. One way that this surface can be constructed is shown in Fig. 2. This surface consists of an infinite number of sheets (A, A_1, A_2, A_3, $\cdots$ and B, B_1, B_2, B_3, $\cdots$). Sheets A and B have an infinite number of branch points and branch cuts; these two sheets are attached by the branch cut along the real axis that connects the branch point $W_{b0} = 0$ to the branch point at infinity. Each of the sheets A_1, A_2, A_3, $\cdots$ and B_1, B_2, B_3, $\cdots$ has only two branch points and one branch cut. Sheet A is attached to each sheet A_i, $i = 1, 2, 3, \cdots$, by the branch cut connecting the branch points W_{ARi} and W_{ALi}.[2] Likewise, sheet B is attached to each sheet B_i, $i = 1, 2, 3, \cdots$, by the branch cut connecting the branch points W_{BRi} and W_{BLi}.

The inverse function $f^{-1}(W)$ maps each sheet of the Riemann surface into a region in the S-plane. The regions in the S-plane corresponding to the sheets in Fig. 2 are shown in Fig. 3. The poles and the zeros of the function $f(S)$ are indicated in Fig. 3 by the crosses and the circles on the imaginary axis, and the points S_{bi} corresponding to the branch points W_{bi} of $f^{-1}(W)$ are indicated by the asterisks. Any two of these regions in the S-plane have at most one point in common (the value of the inverse function at a common branch point). The interconnections of the sheets at the branch cuts are illustrated by the dashed curve on the Riemann surface in Fig. 2. The curve passes through, not over, the cuts. The corresponding curve on the S-plane is shown in Fig. 3; it passes from region to region as the curve on the Riemann surface passes from sheet to sheet. Note, for passive dielectric materials, $\text{Re}(\tilde{\epsilon}_r) \geq 1$ and $\text{Im}(\tilde{\epsilon}_r) \leq 0$; thus the normalized propagation constant S, for real frequencies, must be in the second octant of the S-plane; this is the shaded area in Fig. 3.

In the experimental determination of $\tilde{\epsilon}_r$, the admittance is measured over a range of frequencies which determines a curve in the W-plane, (2). Since W is determined from measured data, it is subject to experimental error. This error can cause the curve in the W-plane to pass onto the wrong sheet when it passes near a branch point. For example, consider the curves C_1 and C_2 on the Riemann surface of the W-plane and on the S-plane in Fig. 4. C_1 is a curve which starts and ends on sheet A. C_2 is a curve displaced by a small amount from C_1; it starts on sheet A but passes onto sheet A_1. Once the curve passes onto the wrong sheet, it is very unlikely that it will return to the correct sheet. The two corresponding curves in the S-plane are very different. One can see that a small error in W that causes the inversion to pass onto the wrong branch (sheet) can cause a large error in S and, therefore, a large error in $\tilde{\epsilon}_r$. In the next section this error is discussed in detail.

An analytical description of the inversion procedure will now be developed. The Riemann surface is a geometric device that can be used to illustrate some of the properties and the problems associated with the inverse. It would be difficult, if not impossible, to form a reasonably simple expression for the inverse on each sheet of the Riemann surface; fortunately, this is not necessary as the following

[2]The subscript $R(L)$ on W indicates that the corresponding point lies in the right (left) half of the S plane.

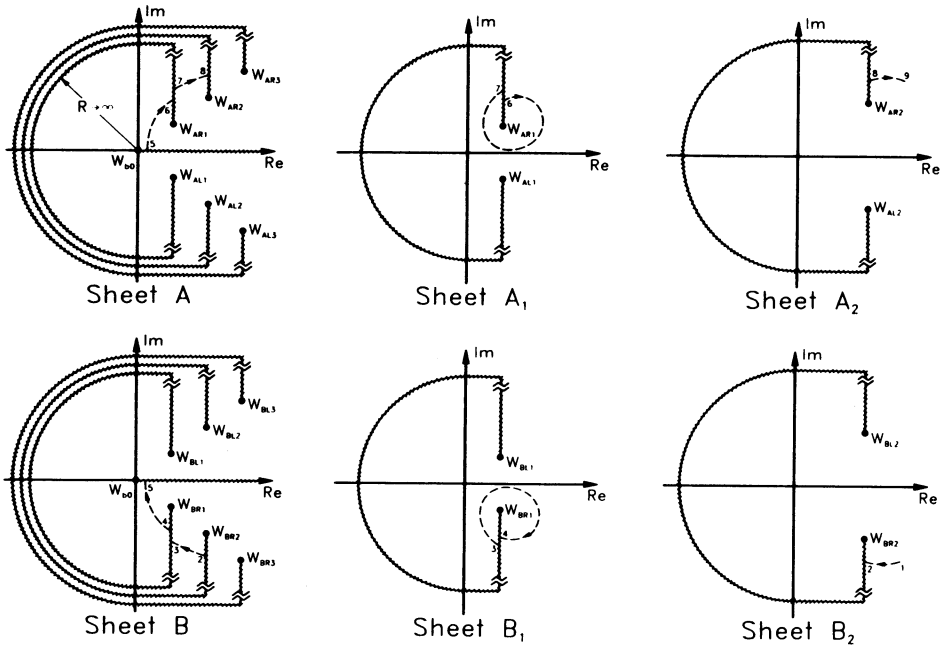

Fig. 2. The Riemann surface of the W-plane (normalized admittance).

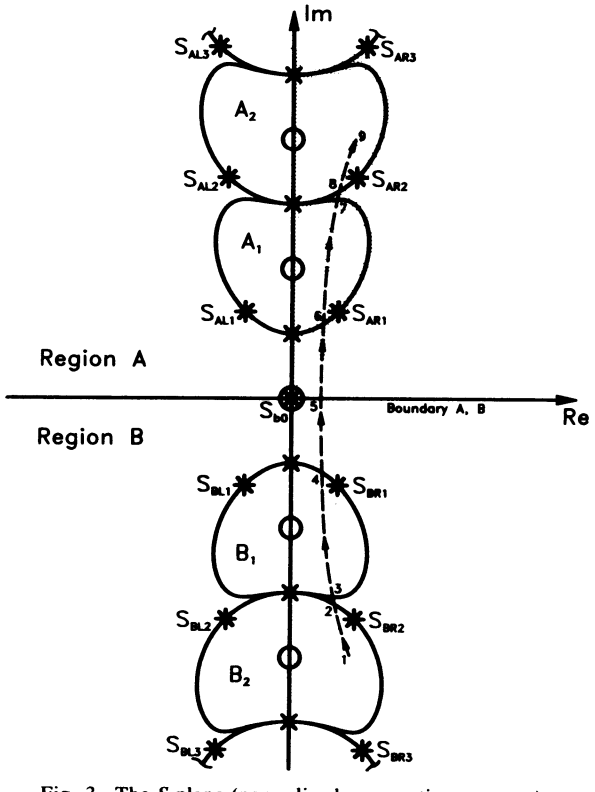

Fig. 3. The S-plane (normalized propagation constant).

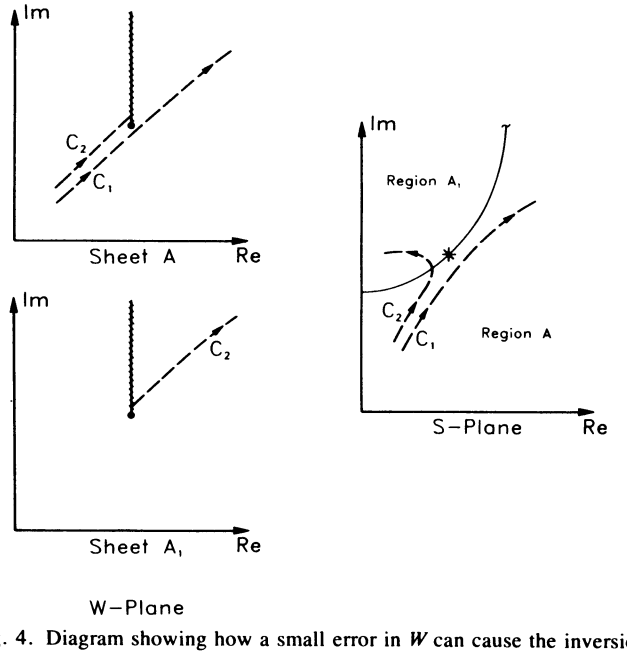

Fig. 4. Diagram showing how a small error in W can cause the inversion to pass onto the wrong branch.

procedure shows. Let C_W be a curve in the W-plane, and let C_S be the corresponding curve in the S-plane that is computed by the inversion procedure. It is assumed that a starting value is given, i.e., the value S_0 corresponding to the measured value W_0.[3] Also, the first derivative of the function f is assumed to be non-zero at the point S_0, i.e., W_0 is not a branch point. The inverse function is expanded in a Lagrange's series about the point W_0 [8]:

$$S = f^{-1}(W) = S_0 + \sum_{n=1}^{\infty} \frac{1}{n!} \left\{ \frac{d^{n-1}}{dS^{n-1}} \left[\frac{S - S_0}{f(S) - W_0} \right] \right\}_{S=S_0} (W - W_0)^n. \quad (7)$$

This representation of f^{-1} is valid whenever $|W - W_0| < \rho$, where ρ is the radial distance on the Riemann surface from W_0 to the closest singularity.

The series in (7) is used to invert a section of the curve in the W-plane that lies within the region where the series is valid. Now, the last point on the section of the curve

[3]One way to obtain a starting value is to make a measurement at a low frequency; then the correct inverse of W_0 is the root of (4) with the smallest magnitude.

C_S, obtained by inverting the section of the curve C_W, can be used as the starting value S_0' for a new Lagrange's series expansion. Repeated application of this procedure produces an analytic continuation of the inverse function f^{-1} from the point S_0. When the curve moves from sheet to sheet on the Riemann surface, the analytic continuation provides an inverse that moves from region to region in the S-plane.

III. Error Analysis

There are several sources of error that occur in the determination of the permittivity $\tilde{\epsilon}_r$ from the measured data. It is assumed that all of these errors can be lumped into an error associated with the measured normalized admittance W. Previously, it was shown how a small error in W can cause a large error in S and in $\tilde{\epsilon}_r$ when the inversion passes onto the wrong branch. This is not the only way an error in W can cause an error in S and in $\tilde{\epsilon}_r$. Even if the inversion is on the correct branch, an error in W will cause an error in S. The inversion process can make the relative error in S either larger or smaller than the relative error in W. In this section these errors are discussed.

The error in S that results from being on the wrong branch is considered first. The value S corresponds to W being on a particular sheet of the Riemann surface, and the value S' corresponds to W being on one of the other sheets of which there are an infinite number. The error that results from being on the wrong branch is then defined as

$$E_B(S) = |S - S'|/|S|. \tag{8}$$

Of the possible values of S', the one that is closest to S is used in (8), so that the error E_B is the minimum error. This error is zero when $W = W_b$, since $S = S' = S_b$, and the error increases as W moves away from W_b, because S and S' move away from S_b and away from each other. The error is easily computed when S and S' are near one of the points S_{bi} (W is near one of the branch points W_{bi}) by using (4) to compute W and S and (11) to compute S' from W. Note that (11) gives two values, S' and the original value of S.

Fig. 5 is a contour graph of the error E_B with S restricted to the first quadrant. Notice that this error is smallest in the regions near the points S_{bi}; these are the regions where it is possible to pass onto the wrong branch. This type of error can be avoided by using a procedure that prevents passage onto the wrong branch when performing the inversion. Such a procedure is presented next.

It is assumed 1) that the path of the curve in the S-plane can be predicted reasonably well from its previous path, and 2) that a reasonable error bound on W is known. Consider the following procedure and the curves C_W and C_S in Fig. 6. First, the analytic continuation is stopped if the error in W can cause the curve C_W to pass on the wrong side of a branch point. The stopping criterion is

$$|W - W_b| < E_W|W| \tag{9}$$

where W is a point on the curve C_W, W_b is the closest

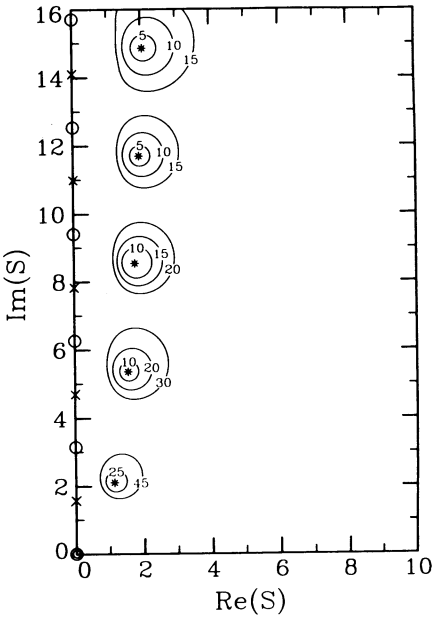

Fig. 5. Contour graph of the error E_B (percent) in S that is the result of the inversion being on the wrong branch. S is restricted to the first quadrant.

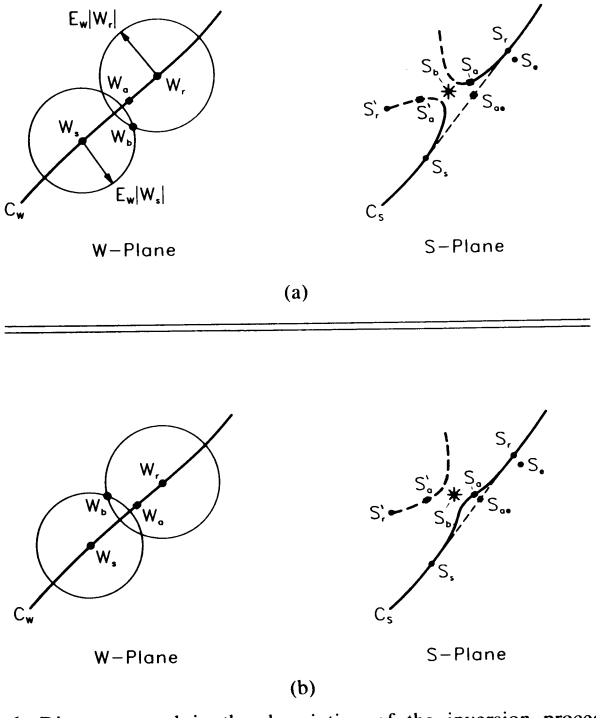

Fig. 6. Diagrams used in the description of the inversion procedure. (a) The error in W causes the curve C_W to pass on the wrong side of the branch point W_b. (b) The curve C_W passes on the correct side of the branch point W_b.

branch point on the Riemann surface, and E_W is the relative error bound on W. This stopping point on C_W is labeled W_s, and the associated point on C_S is S_s. Second, subsequent points along the curve C_W are examined until a point W_r is found where (9) is no longer true. At this point, the value of the inverse S_r is estimated from the previous path of C_S. One way of estimating S_r is by assuming that the value of $\tilde{\epsilon}_r$ does not change very much over the frequency interval associated with skipping from

point W_s to W_r. Using this assumption, the estimate S_e for S_r is

$$S_e = S_s \omega_r / \omega_s \tag{10}$$

where ω_s and ω_r are frequencies associated with S_s and S_r. The next step is to find the one inverse of W_r on each of the two branches that are connected at the branch point W_b. Both of these values can be found by expanding the inverse function f^{-1} in a generalized Lagrange's series about the branch point W_b [8]:[4]

$$S = f^{-1}(W) = S_b + \sum_{n=1}^{\infty} \frac{1}{n!} \left\{ \frac{d^{n-1}}{dS^{n-1}} [\psi(S)] \right\}_{S=S_b} \cdot [\pm (W - W_b)^{1/2}]^n \tag{11}$$

where

$$\psi(S) = \frac{S - S_b}{[f(S) - W_b]^{1/2}}. \tag{12}$$

This representation of f^{-1} is valid whenever $|W - W_b| < \rho$, where ρ is the radial distance on the Riemann surface from the singularity at W_b to the next closest singularity. The two solutions S_r and S_r' are determined by the $\pm$ in (11) when all of the square roots are taken to be on the same branch. Of these two inverses, the one which is closest to the estimated value S_e is chosen.[5] This choice determines which branch the inversion is on.

Now, (11) is used to determine the two possible inverses for each point along the part of the curve C_W that was skipped, for example S_a and S_a' in Fig. 6. Of the two possible inverses, the one S_a closest to a value S_{ae} estimated by linearly interpolating between the point S_s and S_r is chosen:

$$S_{ae} = S_s + (S_r - S_s)(\omega_a - \omega_s)/(\omega_r - \omega_s) \tag{13}$$

where ω_a, ω_s, and ω_r are the frequencies associated with the points S_a, S_s, and S_r, respectively. Finally, the point S_r is used as a starting value to resume the process of analytic continuation. Note that in Fig. 6 two cases are shown (a) the error in W causes the curve C_W to pass on the wrong side of the branch point W_b and (b) the error in W does not cause the curve C_W to pass on the wrong side of the branch point W_b.

The procedure outlined above can be used to invert other functions that have multivalued inverses, for example, the function $f(S) = \tanh(S)/S$ that must be inverted to obtain the permittivity from the measured impedance of a transmission line terminated in a short circuit [9].

This Lagrange's series inversion procedure provides a clear and easily understandable analytic description of the inversion process. A more efficient inversion algorithm was also developed for use with measured data; this algorithm uses a numerical root finding technique and incorporates the procedure described above for choosing the correct branch.

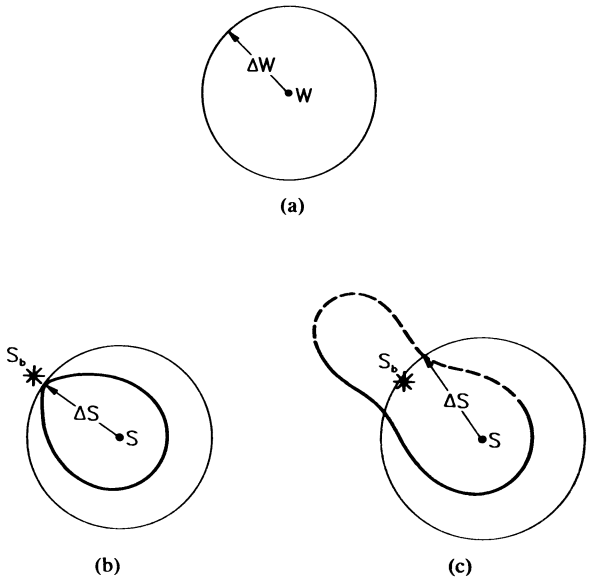

Fig. 7. The vector errors ΔW and ΔS in W and S, respectively.

Now the error in S that results from an error in W is considered. The error in W is represented by the vector ΔW which has a magnitude proportional to the magnitude of W and an arbitrary direction. The addition of W and all of the possible ΔW's defines a circle around the point W, as shown in Fig. 7(a). If the circle does not contain a branch point, the inversion maps the circle into a closed contour around S, as in Fig. 7(b). The upper bound on the error in S is

$$E_S(S) = \underset{W_c}{\text{MAX}} \left| \frac{\Delta S}{S} \right| = \underset{W_c}{\text{MAX}} \left| \frac{S_c - S}{S} \right| \tag{14}$$

where

$$S_c = f^{-1}(W_c)$$

and W_c is a point on the circle around W. If the circle around W contains a branch point, the two branches of the inversion map the circle into two sections of the closed contour around S, the solid and dashed curves in Fig. 7(c). In this case, the upper bound on the error in S is taken to be

$$E_S(S) = \underset{W_c}{\text{MAX}} \left| \frac{\text{MIN}\,[|S_{c1} - S|, |S_{c2} - S|]}{S} \right| \tag{15}$$

where S_{c1} and S_{c2} are the two possible inverses of a point W_c on the circle around W.

Fig. 8 is a contour graph of the error E_S produced by a 2-percent error in the measured normalized admittance ($|\Delta W/W| = 0.02$). In this graph, the regions of highest error surround the points S_{bi}, and the region with the lowest error is adjacent to the imaginary axis. A simple explanation of these errors can be obtained by considering a Taylor series expansion for the function $f(S)$ about a

[4]Here, W_r is assumed to lie within the region of convergence for the series.

[5]It is assumed that the choice between S_r and S_r' is clear. If the choice is not clear, the estimate for S_e (10), is probably not good; or the error-bound E_W is too small.

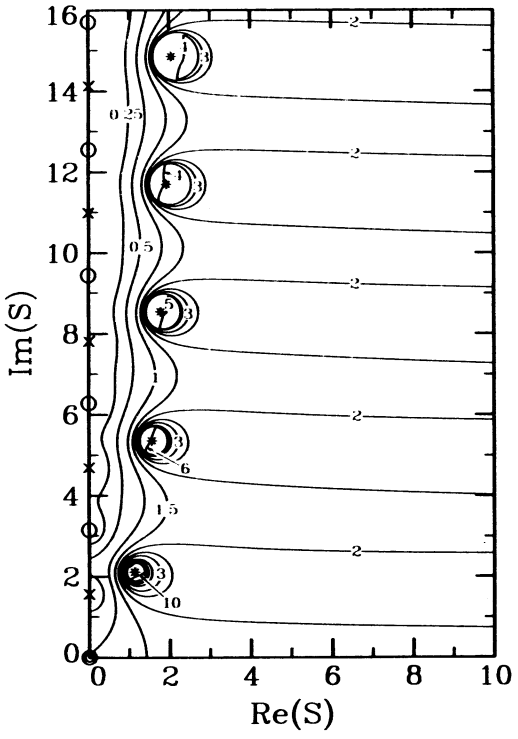

Fig. 8. Contour graph of the error E_s (percent) in the normalized propagation constant produced by a 2-percent error in the normalized input admittance W.

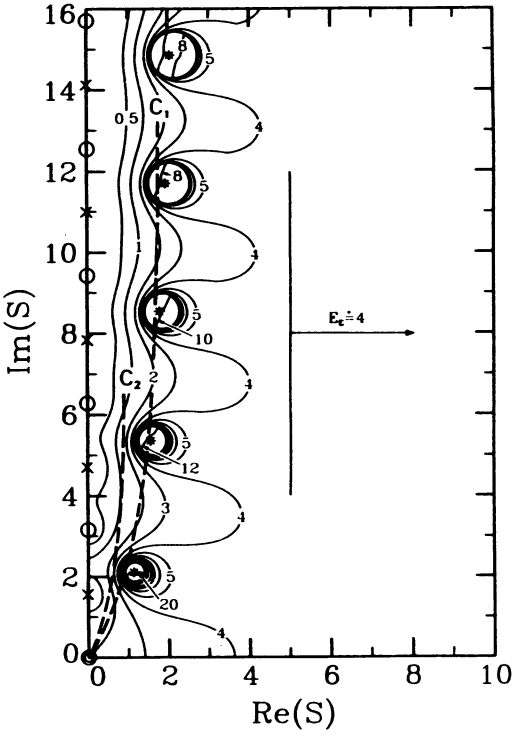

Fig. 9. Contour graph of the error E_ϵ (percent) in the permittivity $\tilde{\epsilon}_r$ produced by a 2-percent error in the normalized input admittance W.

point that is not a singularity of $f(S)$:

$$W + \Delta W = f(S + \Delta S) \approx f(S) + f'(S)\,\Delta S. \quad (16)$$

A rearrangement of (16) gives

$$|\Delta S/S| = M|\Delta W/W| \quad (17)$$

where the multiplier M for the relative error is

$$M \approx |f(S)/Sf'(S)|. \quad (18)$$

In the region adjacent to the imaginary axis, the relative error in S is less then the relative error in W ($M < 1$, $E_S < 2$ percent in Fig. 8) due to the close proximity of the poles and zeros. Near a simple pole or a simple zero S', $M \approx |(S - S')/S| < 1$, and near the double zero at the origin $M \approx 1/2$. In the region surrounding the points S_{bi}, the relative error in S is greater than the relative error in W ($M > 1$, $E_S > 2$ percent in Fig. 8), since $M \approx |1/2(S - S_{bi})| > 1$. In the right half of the graph, the error is approximately constant and equal to 2 percent. This is a consequence of $W = f(S) = S \tanh(S) \approx S$ for Re $(S) \gg 1$ which makes the error in S approximately the same as the error in W.

For the experimenter, a graph of the error E_ϵ in the permittivity due to the error in the measured normalized admittance W is more useful than a graph of E_S. The vector error E_ϵ is determined in the same manner as the error E_S with (14) and (15) replaced by

$$E_\epsilon(S) = \underset{W_c}{\text{MAX}} \left|\frac{\Delta\tilde{\epsilon}_r}{\tilde{\epsilon}_r}\right| = \text{MAX} \left|\frac{S_c^2 - S^2}{S^2}\right| \quad (19)$$

where S_c is the inverse used in (14) or (15).

Fig. 9 is a contour graph of the error E_ϵ for a 2-percent error in W. From this graph, it can be seen that the resulting error in $\tilde{\epsilon}_r$ varies from a minimum of less than 0.5 percent to a maximum of greater than 20 percent depending on the location of S. For an accurate measurement of $\tilde{\epsilon}_r$, it is certainly advantageous to pick the length l of the transmission line so that S for the frequencies of interest remains in the regions of lower error. This point is illustrated in Fig. 9 by the two dashed curves C_1 and C_2 which are for a single material, but for transmission lines of lengths l and $l/2$, respectively. These curves represent the normalized propagation constants measured over the same range of frequencies. C_1 passes through regions of relatively high error, while C_2 passes only through regions of relatively low error.

The relative errors E_s and E_ϵ are determined from the magnitudes of the complex numbers S, ΔS, and $\tilde{\epsilon}_r$, $\Delta\tilde{\epsilon}_r$; their interpretation in terms of vectors is shown in Fig. 7. The relative error in either the real part or the imaginary part of $\tilde{\epsilon}_r = \tilde{\epsilon}_r' - j\tilde{\epsilon}_r''$ can be much larger than the error E_ϵ. This results when there is a large disparity in the size of the two components $\tilde{\epsilon}_r'$ and $\tilde{\epsilon}_r''$.

IV. Measured Permittivities for Primary Alcohols

Measurements were made using several primary alcohols with known permittivities to confirm the inversion procedure and to demonstrate the usefulness of the error analysis. The sample cell shown in Fig. 1 was filled with the alcohol, and a cap was placed on the end of the cell to retain the liquid when the cell was positioned horizon-

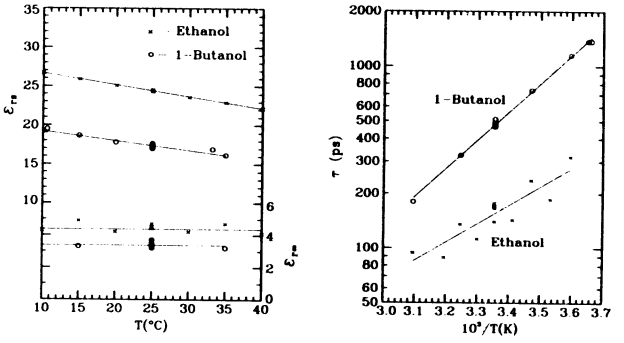

(a) (b)

Fig. 10. (a) Graphs of ϵ_{rs} and $\epsilon_{r\infty}$ as a function of temperature T. (b) Graphs of the relaxation time τ versus $10^3/T$.

tally for the measurement. The cell is formed from a section of 50-Ω Laboratory Precision coaxial air line (General Radio GR900). The center conductor of the line is supported by a Teflon bead of length l_b and relative permittivity $\epsilon_{rb} \approx 2.03$. The input admittance of the sample cell was measured with a time-domain measurement system at frequencies in the range 50 MHz $\leq f \leq$ 2 GHz. This frequency range was determined by the accuracy of the instrumentation. Note that the measurement technique is applicable at any frequency for which the TEM mode is the only propagating mode in the sample cell.

In the previous theoretical analysis, the coaxial transmission line (sample cell) is terminated in a perfect open circuit. The perfect open circuit is a theoretical model, and it can only be approximated in an experiment. When the center conductor of the line is terminated abruptly as in Fig. 1, the input admittance of the transmission line is approximately the same as that for a transmission line that is terminated in a perfect open circuit and has a center conductor that is slightly longer than the physical length $l = l_s + \Delta l$. The additional length Δl has been determined both theoretically and experimentally by several investigators [10]–[12]. For the transmission line used in these experiments $\Delta l \approx 2.4$ mm.[6]

The permittivities of the two alcohols ethanol and 1-butanol are presented in this paper. These alcohols exhibit a Debye relaxation for the complex permittivity over this frequency range [1]:

$$\tilde{\epsilon}_r = \epsilon_r' - j\epsilon_r'' = \epsilon_{r\infty} + (\epsilon_{rs} - \epsilon_{r\infty})/(1 + j\omega\tau). \quad (20)$$

The three parameters ϵ_{rs}, $\epsilon_{r\infty}$, and τ have been measured for these alcohols by many investigators (ethanol [13]–[18] and 1-butanol [13]–[21]). These results are summarized in Fig. 10 where ϵ_{rs} and $\epsilon_{r\infty}$ are graphed as functions of temperature T, and ln (τ) is graphed as a function of $10^3/T$. The graphs of ϵ_{rs} versus T and of ln (τ) versus $10^3/T$ are seen to be approximately straight lines. The temperature dependences of the parameters ϵ_{rs} and τ were estimated by fitting straight lines to the measured data using a least squares error criterion:

$$\epsilon_{rs}(T) = s_0 + s_1 T(C) \quad (21)$$

$$\ln [10^{12}\tau(T)] = r_0 + r_1[10^3/T(K)]. \quad (22)$$

The high frequency permittivity $\epsilon_{r\infty}$ was assumed to be independent of the temperature and equal to the average value of the measured data. The variations $\Delta\epsilon_{rs}$, $\Delta\epsilon_{r\infty}$, and $\Delta\tau$ in the parameters were estimated from the deviation of the measured data from the straight lines near room temperatures (25°C). These variations, the average values of $\epsilon_{r\infty}$, and the coefficients s_0, s_1, r_0, and r_1 are given in Table I for each of the two alcohols.

The measured permittivities of 1-butanol and ethanol are shown in the Argand diagrams in Fig. 11. The solid lines and dashed lines in these graphs represent the measured permittivities of previous investigators. The solid lines were determined from (20) using the parameters ϵ_{rs}, $\epsilon_{r\infty}$, and τ obtained from the values given in Table I. The dashed lines were determined from (20) using the variations $\Delta\epsilon_{rs}$, $\Delta\epsilon_{r\infty}$, and Δ_τ of these parameters. The measured permittivities of both alcohols are seen to be in good agreement with the values measured by other investigators, except for a few of the measured points for ethanol near the top of the semi-circle.

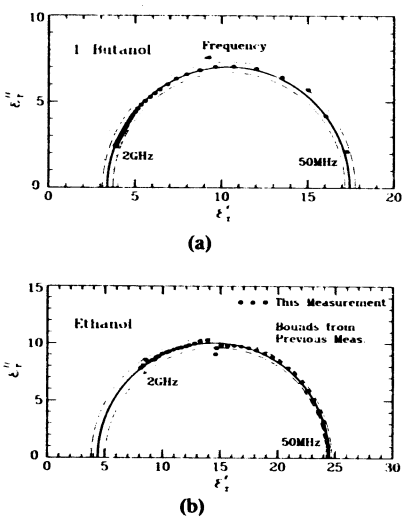

Fig. 11. Argand diagrams of the measured complex permittivity, $T = 24.5 \pm 0.5$°C. (a) 1-Butanol, $l = 13.705$ cm. (b) Ethanol, $l = 6.186$ cm. The spacing between the measured points is 50 MHz.

TABLE I
PARAMETERS OBTAINED FROM THE RESULTS OF PREVIOUS INVESTIGATORS

	ETHANOL	1-BUTANOL
$\Delta\epsilon_{rs}$	±0.2	±0.35
$\Delta\epsilon_{r\infty}$	±0.6	±0.3
$\epsilon_{r\infty}$	4.4	3.4
$\Delta\tau$	± 25 ps	± 35 ps
s_0	28.17	20.45
s_1	−0.1509	−0.1239
r_0	−2.8141	−5.8372
r_1	2.3423	3.5798

[6]If higher frequencies were used, a small additional frequency-dependent term would be included in the expression for Δl. The correction Δl would then depend on the material filling the line.

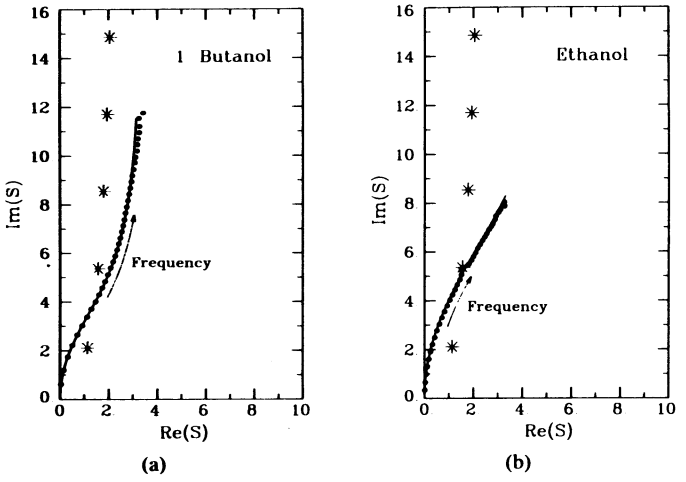

Fig. 12. Graphs of the normalized propagation constant, $T = 24.5 \pm 0.5$°C. (a) 1-Butanol, $l = 13.705$ cm. (b) Ethanol, $l = 6.186$ cm.

The paths of the normalized propagation constants S for the two alcohols ethanol and 1-butanol are shown in Fig. 12. The asterisks indicate the points S_{bi}; recall that the regions of high error surround these points is clearly shown in Fig. 9. The path of the normalized propagation constant for the ethanol, Fig. 12(b), passes very close to one of these points. This is the cause of the increased error in the measured permittivity of the ethanol near the top of the semi-circle in Fig. 11(b). The path of the normalized propagation constant for 1-butanol, Fig. 12(a), does not pass through one of these regions of high error; thus the measured permittivity does not have a region of higher error. At the higher frequencies, the measured values of S for 1-butanol deviate slightly from the solid curve; this is due to the presence of a second relaxation [20], [21].

Note that the frequency range for the measurements presented here was dictated by the available instrumentation. The general measurement technique can be used at all frequencies for which the TEM mode is the only propagating mode in the coaxial sample cell.

VI. Conclusions

The open-circuited coaxial line of general length was studied in detail as a sample cell for broad-band measurements of the dielectric permittivity. The multivalued nature of the inverse function for this cell was discussed. The error that results from passing onto the wrong branch of the inverse function was analyzed, and a procedure that can prevent the passage onto the wrong branch was developed. The measured results demonstrate that the inversion procedure can remain on the correct branch even when a combination of the frequency, sample length, and sample permittivity cause the normalized admittance to pass very close to a branch point of the inverse function.

The error due to the inaccuracies of the instrumentation was also analyzed. Contour graphs were constructed that quantify the effects of this error. The measured results demonstrate that the errors in the permittivity are largest when the normalized input admittance is close to one of the branch points of the inverse function $f^{-1}(W)$, as predicted by the contour graphs.

The error in the measured permittivity can be minimized by adjusting the length of the sample cell so that the path of the normalized propagation constant S lies in a region of low error on these graphs. This length can be determined *a priori* if the permittivity is approximately known. Otherwise, the permittivity can be measured with a cell of convenient length, and then these data used to determine a better cell length, if necessary.

References

[1] A. R. von Hippel, *Dielectric Materials and Applications*. Cambridge, MA: MIT Press, 1954.
[2] S. F. Adam, "A new precision automatic microwave measurement system," *IEEE Trans. Instrum. and Meas.*, vol. IM-17, pp. 308-313, Dec. 1968.
[3] M. J. C. Van Gemert, "High-frequency time-domain methods in dielectric spectroscopy," *Philips Res. Repts.*, vol. 28, pp. 530-572, 1973.
[4] N. S. Nahman, "Picosecond-domain waveform measurements," *Proc. IEEE*, vol. 66, pp. 441-454, Apr. 1978.
[5] W. L. Gans and J. R. Andrews, "Time domain automatic network analyzer for measurement of RF and microwave components," NBS Tech. Note 672, Sept. 1975.
[6] B. Donecker, "Accuracy predictions for a new generation of network analyzer," *Microwave Journal*, vol. 27, no. 6, pp. 127-141, June 1984.
[7] H. E. Bussey, "Dielectric measurements in a shielded open circuit coaxial line," *IEEE Trans. Instrum. Meas.*, vol. IM-29, pp. 120-124, June 1980.
[8] A. I. Markushevich, *Theory of Functions of a Complex Variable*. New York: Chelsea, 1977.
[9] P. M. Morse and H. Feshbach, *Methods of Theoretical Physics*, Part 1. New York: McGraw-Hill, 1953, ch. 4.
[10] P. I. Somlo, "The discontinuity capacitance and the effective position of a shielded open circuit in a coaxial line," in *Proc. I.R.E.E. Australia*, vol. 28, pp. 7-9, Jan. 1967.
[11] B. Bianco, A. Corana, L. Gogioso, and S. Ridella, "Open-circuited coaxial lines as standards for microwave measurements," *Electron. Lett.*, vol. 16, no. 10, pp. 373-374, May 1980.
[12] J. Dibeneditto and A. Uhlir, Jr., "Frequency dependence of 50 Ω coaxial open-circuit reflection standard," *IEEE Trans. Instrum. Meas.*, vol. IM-30, pp. 228-229, Sept. 1981.
[13] J. Peyrelasse, C. Boned, and J. P. LePetit, "Setting up of a time domain spectroscopy experiment. Application to the study of the dielectric relaxation of pentanol isomers," *J. Phys. E: Sci. Instrum.*, vol. 14, pp. 1002-1008, 1981.
[14] A. A. Maryott and E. R. Smith, "Table of dielectric constants of pure liquids," N.B.S. Circular 514, Aug. 1951.
[15] H. Nakamura, S. Mashimo, and A. Wada, "Precise and easy method of TDR to obtain dielectric relaxation spectra in GHz region," *Japanese J. Appl. Phys.*, vol. 21, no. 7, pp. 1022-1024, July 1982.
[16] F. Buckley and A. A. Maryott, "Tables of dielectric dispersion data for pure liquids and dilute solutions," N.B.S. Circular 589, Nov. 1958.
[17] M. W. Sagal, "Dielectric relaxation in liquid alcohols and diols," *J. Chem. Phys.*, vol. 36, no. 9, pp. 2437-2442, May 1962.
[18] A. Suggett, "Time domain methods, Dielectric related molecular processes," *Chem. Soc. London*, vol. 1, pp. 101-120, 1972.
[19] W. Dannhauser and R. H. Cole, "Dielectric properties of liquid butyl alcohols," *J. Phys. Chem.*, vol. 23, no. 10, pp. 1762-1766, Oct. 1955.
[20] A. M. Bottreau, Y. Dutuit, and J. Moreau, "On a multiple reflection time domain method in dielectric spectroscopy: Application to the study of some normal primary alcohols," *J. Chem. Phys.*, vol. 66, no. 8, pp. 3331-3336, Apr. 1977.
[21] R. Chahine and T. K. Bose, "Comparative studies of various methods in time domain spectroscopy," *J. Phys. Chem.*, vol. 72, no. 2, pp. 808-815, Jan. 1980.